

## THE LUMINOSITY FUNCTION AND COSMOLOGICAL EVOLUTION OF X-RAY-SELECTED BL LACERTAE OBJECTS<sup>1,2</sup>

SIMON L. MORRIS

Observatories of the Carnegie Institution of Washington, 813 Santa Barbara Street, Pasadena, CA 91101

JOHN T. STOCKE

Center for Astrophysics and Space Astronomy, University of Colorado, Campus Box 391, Boulder, CO 80309

ISABELLA M. GIOIA,<sup>3</sup> RUDY E. SCHILD, AND ANNA WOLTER<sup>4</sup>

Harvard-Smithsonian Center for Astrophysics, 60 Garden Street, Cambridge, MA 02138

TOMMASO MACCACCARO<sup>5</sup>

Osservatorio Astronomico di Bologna, via Zamboni 33, I-40126 Bologna, Italy

AND

ROBERTO DELLA CECA

Dipartimento di Astronomia, Università di Bologna, via Zamboni 33, I-40126 Bologna, Italy

Received 1990 December 26; accepted 1991 April 23

### ABSTRACT

We present redshifts for an X-ray-selected, flux-limited sample of BL Lac objects. We derive a median X-ray luminosity of  $10^{49.83}$  W Hz<sup>-1</sup>. We also find a correlation between the optical and radio luminosity of these objects. The complete redshift information allows measurement of the objects' evolution with redshift and calculation of a luminosity function at zero redshift. We find evidence for strong "negative" evolution (BL Lac objects were either less common or less luminous in the recent past). We discuss the differences between radio- and X-ray-selected samples of BL Lac objects, and suggest that X-ray selection picks out chiefly beamed FR I radio galaxies, while radio selection finds a mix of beamed and microlensed quasars, along with extreme examples of beamed FR I radio galaxies.

*Subject Headings:* BL Lacertae objects — galaxies: nuclei — galaxies: redshifts — X-rays: sources

### 1. INTRODUCTION

BL Lacertae objects are an enigmatic class of active galaxies. They have been studied intensively for more than 10 years (see Wolfe 1978 and Maraschi, Maccacaro, & Ulrich 1989 for two comprehensive summaries of the field), but there is still no universally accepted model for these objects (or even universally accepted observational criteria defining the class). In this paper we describe a sample of objects drawn from the *Einstein* Medium-Sensitivity Survey (EMSS) which satisfy most criteria for classification as BL Lac objects. For the first time we are able to obtain almost complete redshifts for a well-defined sample of BL Lac objects and hence derive luminosity distributions and also the evolution of the class and its luminosity function.

The EMSS is a sample of 835 serendipitous X-ray sources from *Einstein* imaging proportional counter (IPC) images; see Gioia et al. (1990a) and Stocke et al. (1991) for details on the X-ray and optical properties of the sample. The selection criteria for classification as an EMSS BL Lac object are given in

Stocke et al. (1991), and discussed in some detail there; to summarize here, they are the following:

1. Inclusion in the EMSS sample of serendipitous X-ray sources.
2. Equivalent width (EW) of any emission lines less than 5 Å.
3. Evidence for dilution of starlight in the spectrum by a nonthermal continuum. In practice this was taken as a requirement that the Ca II break, if present, had a "contrast" of less than 25% in our identification spectra.

The last two criteria are meant to separate out "featureless" objects, and are not based on any physical model of the objects. The spectroscopic data upon which the original BL Lac classification was based were taken at the MMT and the LCO du Pont telescope. The typical wavelength coverage for these spectra is 3400–6400 Å with a resolution of 7 Å. It should be noted that we do not impose any polarization criteria. Strong optical polarization is often taken as a requirement for classification as a BL Lac object. Polarization data have been taken for 22 of the EMSS BL Lac sample, and 14 have shown polarization above 3% (Elston, Jannuzi, & Smith 1989; Jannuzi 1990). Many of the objects in our sample not yet detected polarimetrically are too faint to allow detection of weak polarization. We do not feel that relaxing the requirement of strong optical polarization invalidates our classification of these as BL Lac objects, since they possess all the other common properties of the class (featureless optical spectra, variable flux in the optical, strong X-ray emission, radio emission). In fact, many samples of BL Lac objects constructed to date have been defined spectroscopically, and only later observed polarimetrically (e.g., Kühr & Schmidt 1990).

<sup>1</sup> Observations were primarily made at Palomar Observatory as part of a collaborative agreement between the California Institute of Technology and the Carnegie Institution of Washington.

<sup>2</sup> This paper uses some data obtained at the Multiple Mirror Telescope Observatory (MMTO), which is operated jointly by the University of Arizona and the Smithsonian Institution.

<sup>3</sup> Also from Istituto di Radioastronomia del CNR, via Irnerio 46, I-40126 Bologna, Italy.

<sup>4</sup> Also from Osservatorio Astronomico di Brera, via Brera 28, I-20121 Milano, Italy.

<sup>5</sup> Also from Harvard-Smithsonian Center for Astrophysics, 60 Garden Street, Cambridge, MA 02138.

It is common in the literature to consider highly polarized quasars (HPQs) to be closely related to BL Lac objects, and to call the two merged groups “blazars.” We note that 24 of the radio-loud active galactic nuclei (AGNs) in the EMSS have been observed polarimetrically, and no example has yet been found of an HPQ in the EMSS (Jannuzi 1990). We will discuss this further in § 4.2.1.

In order to derive a luminosity function for the EMSS BL Lac objects, we construct a “complete” sample with the following further constraints:

4. X-ray flux of  $5 \times 10^{13}$  ergs  $\text{cm}^{-2}$   $\text{s}^{-1}$  or more (0.3–3.5 keV).
5. Declination of  $-20^\circ$  or higher.

These last two constraints mean that the BL Lacs are drawn from a sample of X-ray-selected objects that are fully identified, and biases can only be introduced by misidentification of an X-ray source. We will refer to this sample as the complete EMSS sample of BL Lac objects. There are 22 objects in this sample. We note that all of the EMSS BL Lac objects in the complete sample have been observed with the VLA, and all are detected as radio sources (see Stocke et al. 1990).

Several studies of the properties of our sample of BL Lac objects have been published. Maccacaro et al. (1984b) showed that the BL Lac number counts were flatter than a Euclidean prediction. Stocke et al. (1985) looked at the overall energy distributions of X-ray-selected BL Lac objects and showed that there were systematic differences between X-ray- and radio-selected BL Lac objects, with X-ray-selected objects having a larger fraction of starlight in their spectrum, being less variable, and being less highly polarized. Maccacaro et al. (1989) and Wolter et al. (1991a) updated the results of Maccacaro et al. (1984b) and derived more detailed constraints on the BL Lac luminosity function and evolution from the number counts. Stocke et al. (1990) showed that there were no objects in the EMSS which could be called “radio-quiet” BL Lac objects, i.e., satisfying all the criteria above but with no detectable radio emission.

In § 2 we describe the new observations used in this paper. In § 3 we present the analysis of the data: redshift determination, calculation of luminosities and correlation analysis, and determination of the luminosity function. We discuss these results in § 4, and present our conclusions in § 5. The spectra for individual objects are described in the Appendix.

Throughout this paper, luminosities are calculated assuming  $H_0 = 50 \text{ km s}^{-1} \text{ Mpc}^{-1}$  and  $q_0 = 0.0$ .

## 2. OBSERVATIONS AND REDUCTION

The new observations presented in this paper were made over an 8 month period during three observing runs at the 5 m Hale Telescope on Palomar Mountain. A log of these observations is presented in Table 1. The run on 1989 June was chiefly for a different observing project, and so the spectrograph setup differs slightly from that of the 1988 November and 1989 April runs. The double spectrograph was used with a dichroic splitting the spectra at  $\sim 5000 \text{ \AA}$  for the 1988 November and 1989 April runs, and at  $\sim 5400 \text{ \AA}$  for the 1989 June run. A 300 line  $\text{mm}^{-1}$  grating was used on the blue side, giving a dispersion of 2.17  $\text{\AA}$  per CCD pixel and (with a 1" slit) a resolution (FWHM) of 6  $\text{\AA}$ . On the red side a 158 line  $\text{mm}^{-1}$  grating gave a dispersion of 6.07  $\text{\AA}$  per CCD pixel and a resolution of 18  $\text{\AA}$ . During the 1988 November and 1989 April runs the grating angles were set to give coverage from 3400 to 5100  $\text{\AA}$  in the blue and

TABLE 1  
LOG OF OBSERVATIONS

Object	Date	Exposure (minutes)	Figure 1 Reference
MS 0122.1 + 0903.....	1988 Nov 14–16	60	A
MS 0158.5 + 0019.....	1988 Nov 14–16	90	B
MS 0205.7 + 3509.....	1988 Nov 14–16	120	C
MS 0256.9 + 3429.....	1988 Nov 14–16	60	D
MS 0419.3 + 1943.....	1988 Nov 14–16	180	E
MS 0607.9 + 7108.....	1988 Nov 14–16	70	F
MS 0607.9 + 7108.....	1989 Apr 3–5	60	G
MS 0737.9 + 7441.....	1988 Nov 14–16	60	H
MS 0737.9 + 7441.....	1989 Apr 3–5	60	I
MS 0922.9 + 7459.....	1988 Nov 1416	90	J
MS 0922.9 + 7459.....	1989 Apr 3–5	60	K
MS 0950.9 + 4929.....	1988 Nov 14–16	90	L
MS 0950.9 + 4929.....	1989 Apr 3–5	60	M
MS 0958.9 + 2102.....	1989 Apr 3–5	90	N
MS 1207.9 + 3945.....	1989 Apr 3–5	180	O
MS 1221.8 + 2452.....	1989 Apr 3–5	60	P
MS 1402.3 + 0416.....	1089 Apr 3–5	100	Q
MS 1407.9 + 5954.....	1989 Apr 3–5	150	R
MS 1443.5 + 6349.....	1989 Apr 3–5	180	S
MS 1458.8 + 2249.....	1989 Apr 3–5	60	T
MS 1534.2 + 0148.....	1989 Apr 3–5	100	U
MS 1704.9 + 6046.....	1988 Nov 14–16	60	V
MS 1757.7 + 7034.....	1988 Nov 14–16	150	W
MS 1757.7 + 7034.....	1989 Jun 27	60	X
MS 2143.4 + 0704.....	1988 Nov 14–16	40	Y
MS 2143.4 + 0704.....	1989 Jun 27	60	Z

from 4900 to 9400  $\text{\AA}$  in the red. In 1989 June coverage from 3800 to 5500  $\text{\AA}$  in the blue and from 5300 to 9800  $\text{\AA}$  in the red was obtained.

The spectra were extracted using the optimal extraction routines in the IRAF<sup>6</sup> APEX TRACT package. Flux calibration was performed using wide-slit observations of flux standards, and no correction was made for light loss on the slit jaws. The seeing was rather variable during the 1988 November run, and so the derived fluxes are probably uncertain by a factor of  $\sim 2$  or less. Several of the objects were observed more than once during a run, and these data were combined to produce the final spectrum, so the fluxes should be considered averages over the run. Also, several objects were observed in two different runs. In general these spectra were not combined but were used separately to confirm the reality of weak features. The narrow-slit and changeable conditions make any attempt to study the variability of these objects from our spectra pointless. Photometric monitoring of these targets is being carried out by one of us (R. S.). For each spectrum a  $1 \sigma$  noise estimate based on Poisson statistics was also created and carried through the reduction procedure, and hence the red and blue data could be combined using variance weighting in the overlap region to produce the spectra shown in Figures 1a–1z. The spectra shown have been smoothed with a Gaussian of FWHM 9  $\text{\AA}$ . The noise spectra have not been modified to account for the smoothing, i.e., they are an estimate of the uncertainty in each pixel in the unsmoothed data. In studying the spectra the reader should be warned that the joining procedure between the blue and red spectra often created features in the spectra at the join wavelength. The location of these spurious features can be identified from the noise spectra which show a discontinuity at the join. The strong atmospheric absorption feature

<sup>6</sup> IRAF is distributed by NOAO, which is operated by AURA, Inc., under contract to the NSF.

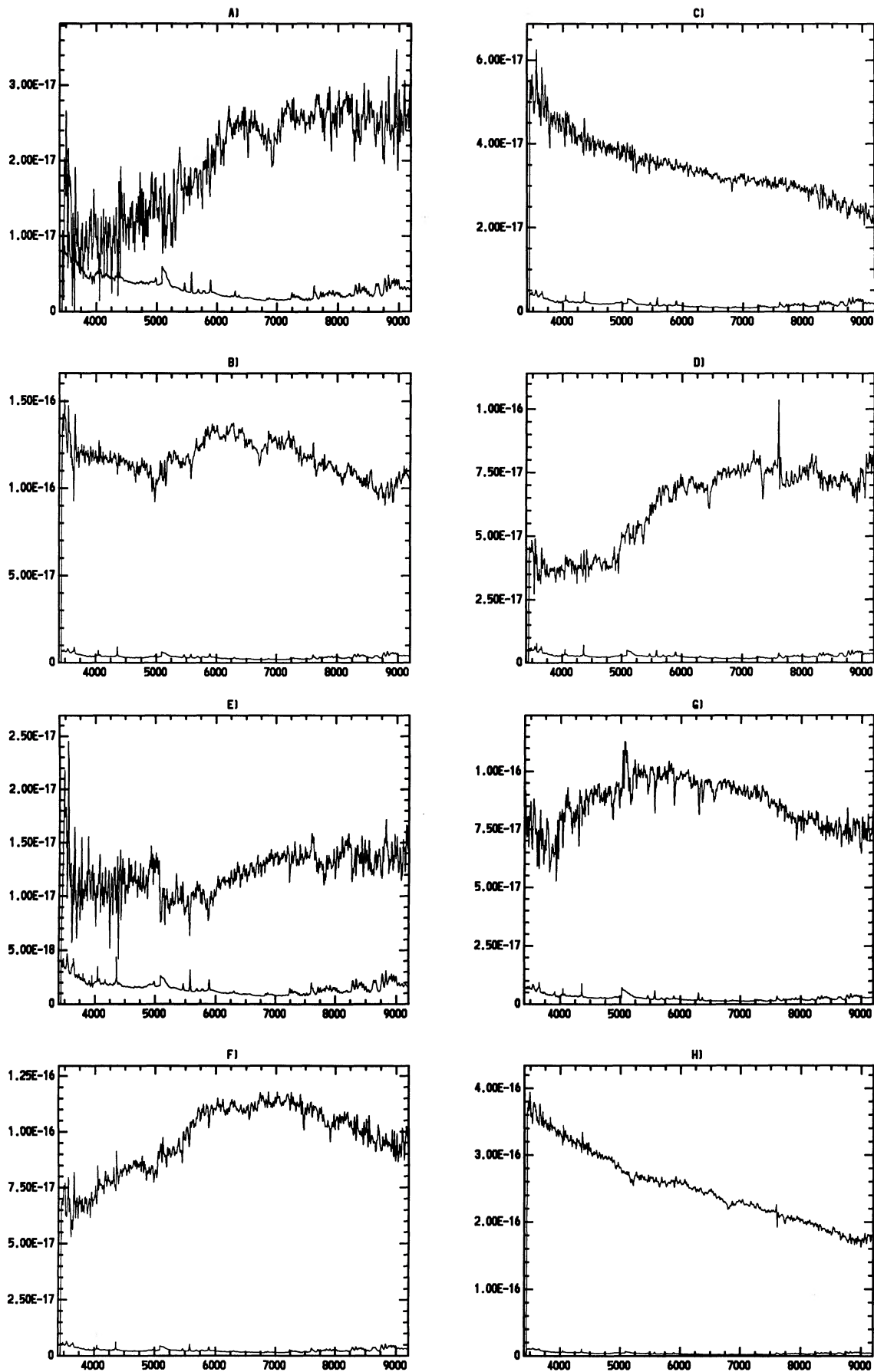


FIG. 1.—(a-z) Palomar 200 inch (5.08 m) spectra of EMSS BL Lac objects. Spectra shown are in the same order as given in Table 1. Flux scale is  $F_{\lambda}$  in  $\text{ergs cm}^{-2} \text{s}^{-1} \text{\AA}^{-1}$ ; the x-axis is the wavelength in  $\text{\AA}$ . Plotted below each spectrum is an estimate of the  $1 \sigma$  uncertainty.

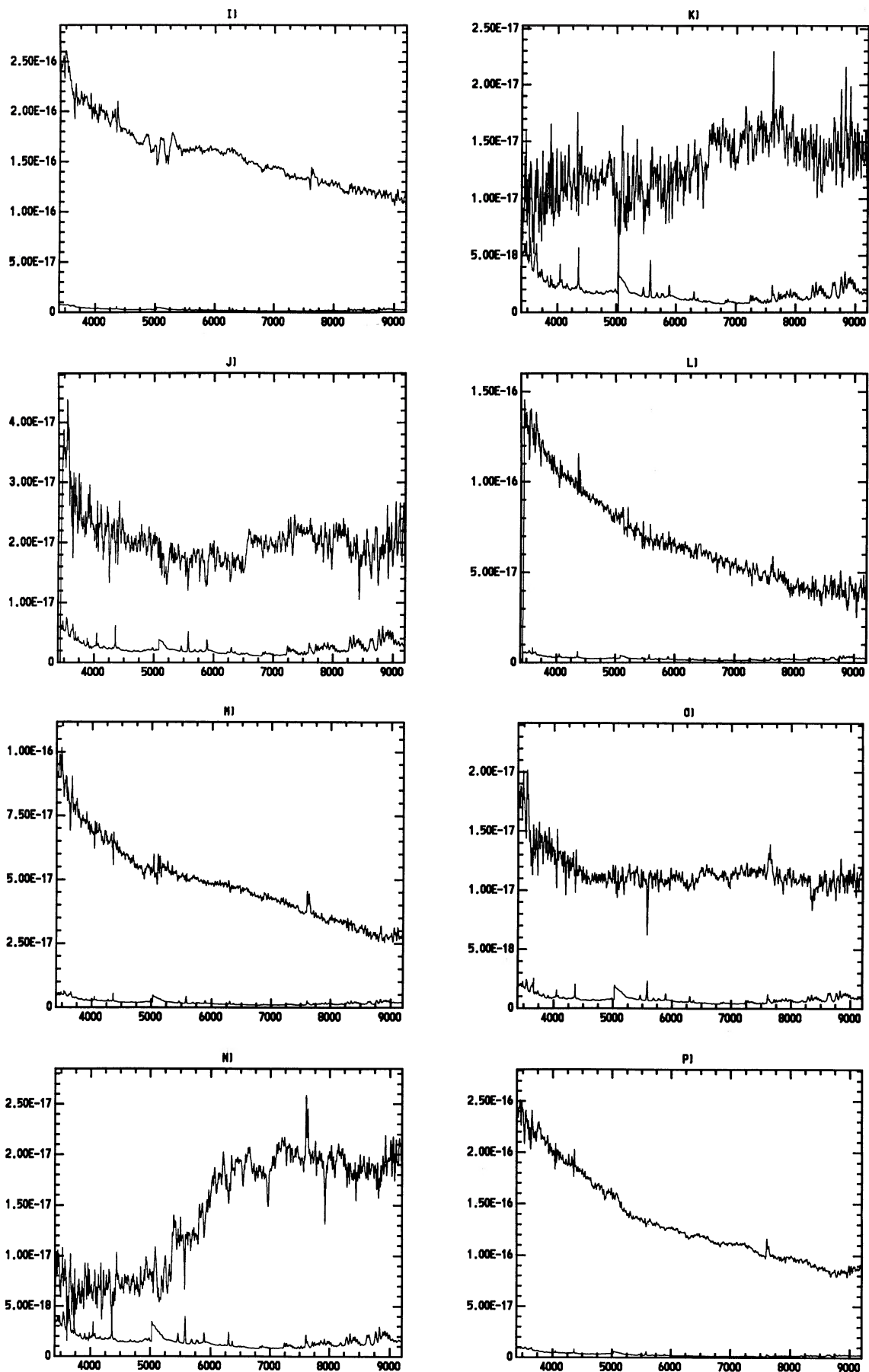


FIG. 1—Continued

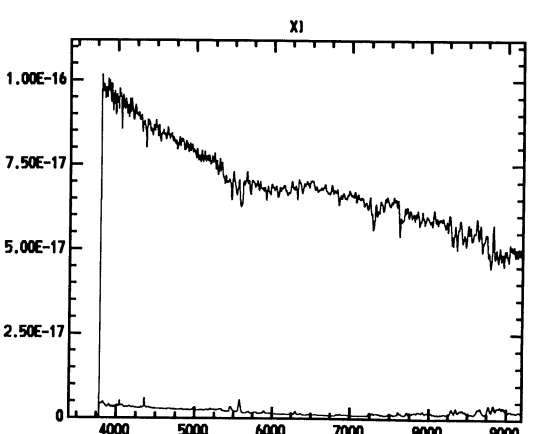
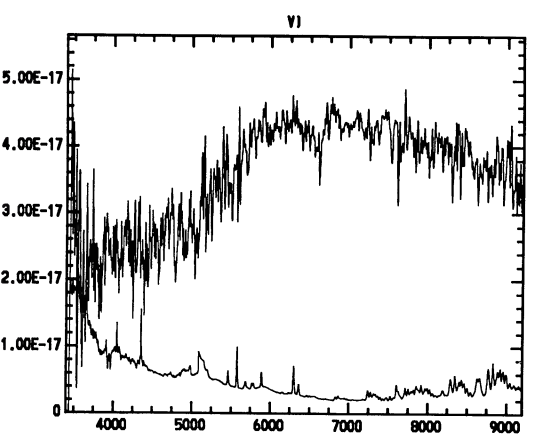
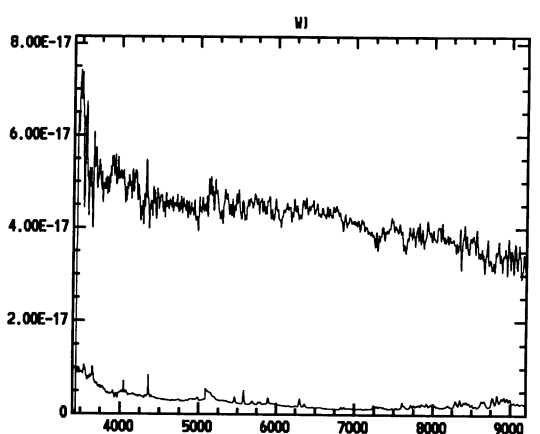
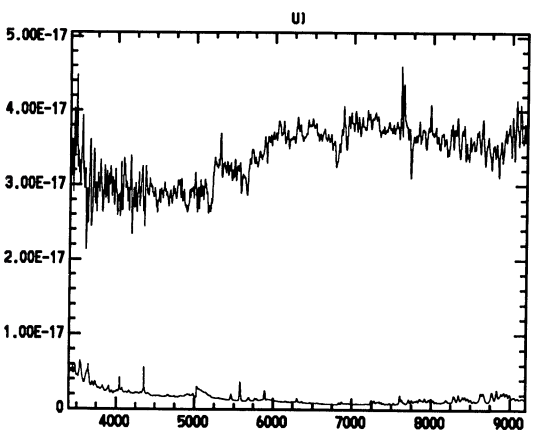
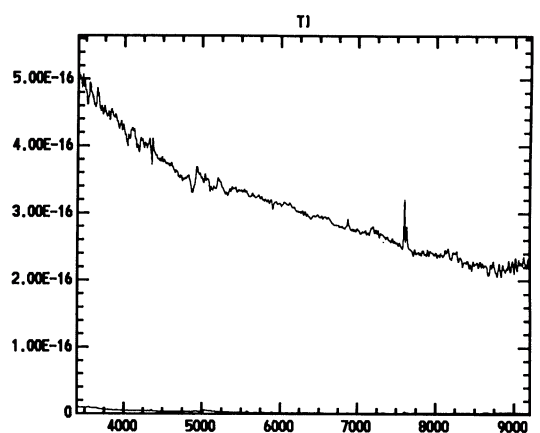
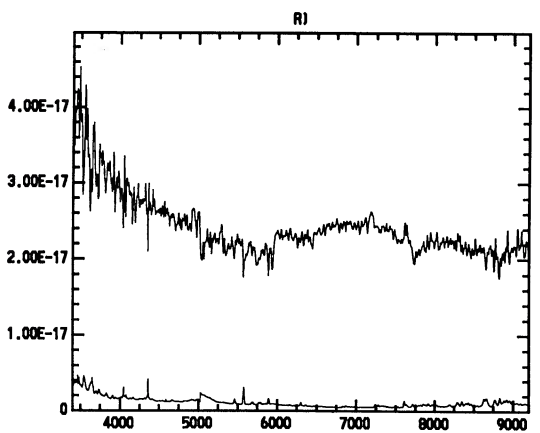
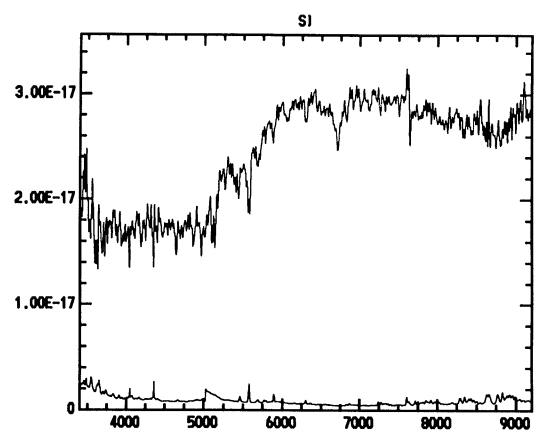
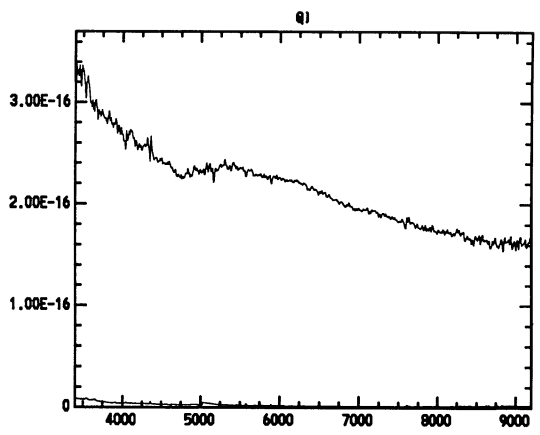


FIG. 1—Continued

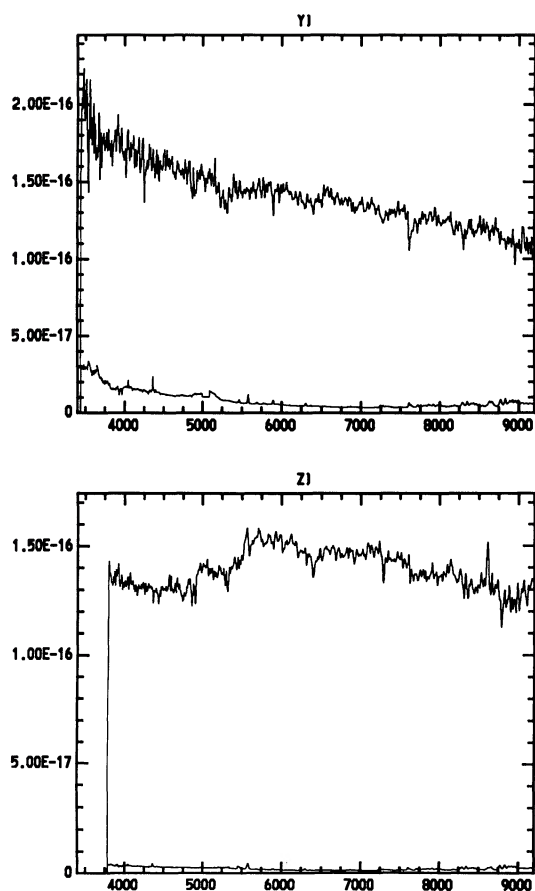


FIG. 1—Continued

due to  $O_2$  at  $7600 \text{ \AA}$  also often leaves a spurious feature in the spectra.

### 3. ANALYSIS

The Palomar data had two main uses first, to confirm that the spectra match the EMSS criteria for a BL Lac object (Stocke et al. 1991 and § 1 above) and, second, to allow redshift estimation. Three objects observed at Palomar (MS 0036.5 + 2103, MS 0815.7 + 5233, and MS 0850.2 + 2825) were shown to have emission lines stronger than our  $5 \text{ \AA}$  cutoff and hence do not satisfy our BL Lac classification criteria. We will not consider these three weak-lined quasars further herein, but they are discussed in Stocke et al. (1991).

#### 3.1. Redshift Determination

Considerable thought was given to the process of deriving redshifts from noisy spectra with weak features. Clearly, if a good template were available, some form of cross-correlation would be best, being both objective and simple to perform. Unfortunately, a number of factors make this approach unreliable and subjective except in those cases where a redshift is already obvious from visual inspection.

1. A BL Lac template does not exist. The spectra are made up of starlight plus a nonthermal continuum of unknown shape.

2. In objects with a strong nonthermal continuum, systematic errors in the flux calibration, and a poor join between the

blue and red halves of the spectrum, may dominate any real features in the continuum.

3. If the nonthermal continuum could be removed, leaving only starlight, a template elliptical galaxy would presumably work well. Unfortunately, removal of the nonthermal continuum prior to analysis requires some knowledge of the redshift (to determine a fitting window away from strong starlight contributions—in practice shortward of  $4000 \text{ \AA}$  in the BL Lac rest frame) and an assumption that the nonthermal continuum shape is well represented by some simple analytic shape (e.g., a power law).

A number of tests were made using the IRAF Fourier analysis software, using both the raw spectra and spectra in which a power-law fit was subtracted, resulting in the conclusion that redshift determination by visual inspection of the spectra was in fact more reliable than any cross-correlation technique for this somewhat heterogeneous sample of spectra.

The new redshifts quoted in Table 2 were thus derived by visual inspection of the spectra plotted in Figure 1. For completeness, redshifts of EMSS BL Lac objects which were not determined from Palomar data are also included (an updated version of the list in Maccacaro et al. 1989). Redshifts were assigned to three confidence categories: *firm*: at least three

TABLE 2  
REDSHIFTS OF EMSS BL LAC SAMPLE

Object	Sample <sup>a</sup>	Redshift	Confidence <sup>b</sup>
MS 0122.1 + 0903.....	C	0.339	F
MS 0158.5 + 0019.....	C	0.299	F
MS 0205.7 + 3509.....	C	0.318	T
MS 0257.9 + 3429.....	C	0.247	F
MS 0317.0 + 1834.....	C	0.190	F
MS 0331.3 - 3629.....	...	0.308	F
MS 0350.0 - 3712.....	...	0.165	F
MS 0419.3 + 1943.....	C	0.512	T
MS 0607.9 + 7108.....	C	0.267	F
MS 0622.5 - 5256.....	...	...	...
MS 0737.9 + 7441.....	C	0.315	F
MS 0922.9 + 7459.....	C	0.638	T
MS 0950.9 + 4929.....	C	0.207	P
MS 0958.9 + 2102.....	...	0.344	F
MS 1133.7 + 1618.....	...	...	...
MS 1207.9 + 3945.....	C	0.615	F
MS 1221.8 + 2452.....	C	0.218	P
MS 1229.2 + 6430.....	C	0.164	F
MS 1235.4 + 6315.....	C	0.297	F
MS 1256.3 + 0151.....	...	...	...
MS 1258.4 + 6401.....	...	...	...
MS 1312.1 - 4221.....	...	0.108	F
MS 1332.6 - 2935.....	...	0.256	P
MS 1402.3 + 0416.....	C	0.200	P
MS 1407.9 + 5954.....	C	0.495	F
MS 1443.5 + 6349.....	C	0.299	F
MS 1458.8 + 2249.....	C	0.235	T
MS 1534.2 + 0148.....	C	0.312	F
MS 1552.1 + 2020.....	C	0.222	F
MS 1704.9 + 6046.....	...	0.280	F
MS 1757.7 + 7034.....	C	0.407	F
MS 2143.4 + 0704.....	C	0.237	F
MS 2306.1 - 2236.....	...	0.137	F
MS 2336.5 + 0517.....	...	...	...
MS 2342.7 - 1531.....	...	...	...
MS 2347.4 + 1924.....	...	0.515	F

<sup>a</sup> C indicates the object is a member of the EMSS complete sample.

<sup>b</sup> F: firm, T: tentative, P: possible. See Appendix and Fig. 1.

stellar absorption features were seen with a consistent redshift (always three of Ca II, the G band, Mg *b*, or Na D) and a continuum shape consistent with this redshift (i.e., a break at the Ca II wavelength and an excess over a power-law fit redward of this); *tentative*: at least two stellar absorption features with a consistent redshift; *possible*: a redshift based on very uncertain criteria, such as a break in the continuum shape which could be the 4000 Å feature or a redshift with features which are not consistent. The uncertain cases were also checked for consistency with the original MMT classification spectra. Comments for each object are listed in the Appendix. Four of the BL Lacs in the EMSS complete sample were not observed at Palomar, since their redshifts were known from MMT observations. The spectra of these objects can be found in Stocke et al. (1985) and Stocke et al. (1989). Figure 2 shows the redshift distribution for the complete EMSS BL Lac sample. We should emphasize that this redshift distribution can only be compared with the predictions of any luminosity function model after that model has been convolved through the EMSS sky coverage as a function of flux; see § 3.3.1 and Table 6.

### 3.2. Fluxes and Luminosities

Table 3 contains the observed fluxes and luminosities for the EMSS complete sample of BL Lac objects. The fluxes are given in the observed form and are then converted to monochromatic luminosities at a fixed rest frequency in the frame of the BL Lac. For this conversion the X-ray flux was assumed to have a power-law dependence on frequency:

$$F_\nu = F_{\nu_0} \left( \frac{\nu}{\nu_0} \right)^\alpha \quad (1)$$

with  $\alpha = -1$ . This spectral index is the mean observed for a sample of X-ray-selected BL Lac objects studied by Worrall & Wilkes (1990), and is also the mean for the EMSS combined sample of AGNs and BL Lac objects (Maccacaro et al. 1988). Due to the low total counts and off-axis position of the EMSS BL Lac X-ray data on the IPC, it is not possible to measure individual X-ray spectral indices from our *Einstein* IPC detections. *ROSAT* PSPC observations are in progress to check this

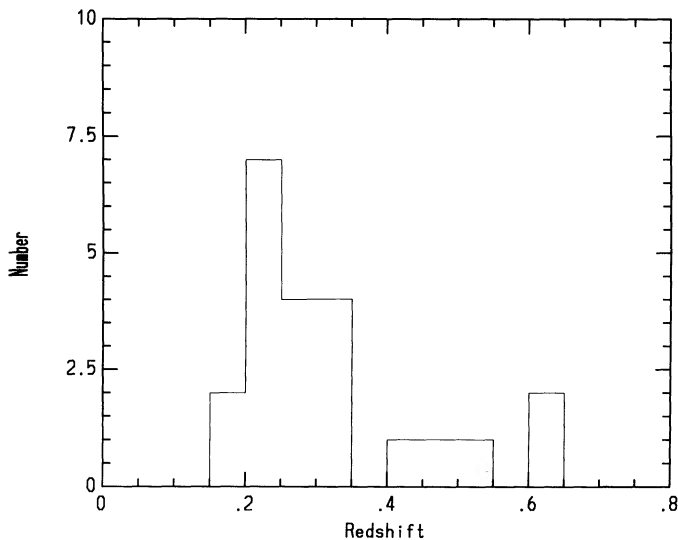


FIG. 2.—Redshift distribution for the complete EMSS BL Lac sample

TABLE 3  
FLUXES AND LUMINOSITIES OF COMPLETE EMSS BL LAC SAMPLE

Name	$F_x^a$	$F_o^b$	$F_r^c$	$L_x^d$	$L_o^e$	$L_r^f$
MS 0122.1+0903.....	7.42	19.98	1.4	19.63	22.53	23.85
MS 0158.5+0019.....	86.92	17.96	11.3	20.57	23.20	24.65
MS 0205.7+3509.....	5.24	19.24	3.6	19.41	22.79	24.20
MS 0257.9+3429.....	12.32	18.53	10.0	19.54	22.92	24.42
MS 0317.0+1834.....	123.74	18.12	17.0	20.29	22.78	24.43
MS 0419.3+1943.....	25.47	20.26	8.0	20.58	23.35	24.97
MS 0607.9+7108.....	13.04	19.60	18.2	19.64	22.58	24.75
MS 0737.9+7441.....	97.51	16.89	24.0	20.67	23.69	25.02
MS 0922.9+7459.....	10.79	19.74	3.3	20.44	23.37	24.79
MS 0950.9+4929.....	20.75	19.30	3.3	19.59	22.28	23.79
MS 1207.9+3945.....	14.80	19.12	5.8	20.54	23.57	25.00
MS 1221.8+2452.....	12.49	17.65	26.4	19.42	22.99	24.74
MS 1229.2+6430.....	33.73	16.89	42.0	19.59	23.00	24.69
MS 1235.4+6315.....	18.64	18.59	7.0	19.90	22.98	24.43
MS 1402.3+0416.....	11.19	17.08	20.8	19.29	23.13	24.56
MS 1407.9+5954.....	19.83	19.67	16.5	20.44	23.13	25.26
MS 1443.5+6349.....	15.97	19.65	11.6	19.83	22.52	24.66
MS 1458.8+2249.....	10.50	16.79	29.8	19.42	23.41	24.86
MS 1534.2+0148.....	20.59	18.70	34.0	19.98	22.95	25.16
MS 1552.1+2020.....	43.02	17.70	37.5	19.98	22.99	24.91
MS 1757.7+7034.....	23.44	18.27	7.2	20.31	23.46	24.72
MS 2143.4+0704.....	22.17	18.04	50.0	19.75	22.96	25.09

<sup>a</sup> Observed X-ray flux in units of  $1.0 \times 10^{-13}$  ergs  $\text{cm}^{-2}$   $\text{s}^{-1}$  in 0.3–3.5 keV energy band.

<sup>b</sup> *V*-magnitude.

<sup>c</sup> 6 cm radio flux in mJy.

<sup>d</sup> Logarithm of the monochromatic X-ray luminosity at 2 keV in the BL Lac rest frame in  $\text{W Hz}^{-1}$ .

<sup>e</sup> Logarithm of the monochromatic optical luminosity at 5500 Å in the BL Lac rest frame in  $\text{W Hz}^{-1}$ .

<sup>f</sup> Logarithm of the monochromatic radio luminosity at 6 cm in the BL Lac rest frame in  $\text{W Hz}^{-1}$ .

assumption. A rest frequency of 2 keV was chosen. For the optical, *V*-magnitudes were converted to monochromatic luminosities at 5500 Å, assuming that the flux for a zeroth magnitude object is  $3.67 \times 10^{-23}$   $\text{W m}^{-2}$   $\text{Hz}^{-1}$ , and assuming a power-law index  $\alpha = -2$  (Wills 1989; see also Fig. 1). In the radio, a power-law index of zero was assumed (this assumption is being tested by VLA observations of several of the sample; Wolter et al. 1991b; see also Stocke et al. 1985). Median, mean, and rms values for the EMSS complete BL Lac sample are given in Table 4. The luminosity distributions are shown in Figure 3. It should be noted that the luminosities quoted assume that the BL Lac flux is being radiated isotropically, an assumption which is probably incorrect but which is useful when comparing BL Lac objects to other classes of objects, and models in the literature.

A correlation analysis was performed for the fluxes and luminosities of the EMSS complete BL Lac sample. This analysis included the logarithm of the proper distance, in order to check for correlations with distance (due to either selection effects or evolution). Table 5 lists the percentage probabilities

TABLE 4  
MEDIANS, MEANS AND rms OF EMSS BL LAC  
SAMPLE LUMINOSITIES (22 objects)<sup>a</sup>

Parameter	Median	Mean	rms
$L_x$ .....	19.82	19.95	0.46
$L_o$ .....	22.99	22.03	0.36
$L_r$ .....	24.72	24.68	0.38

<sup>a</sup> Parameters are the same as those in Table 3.

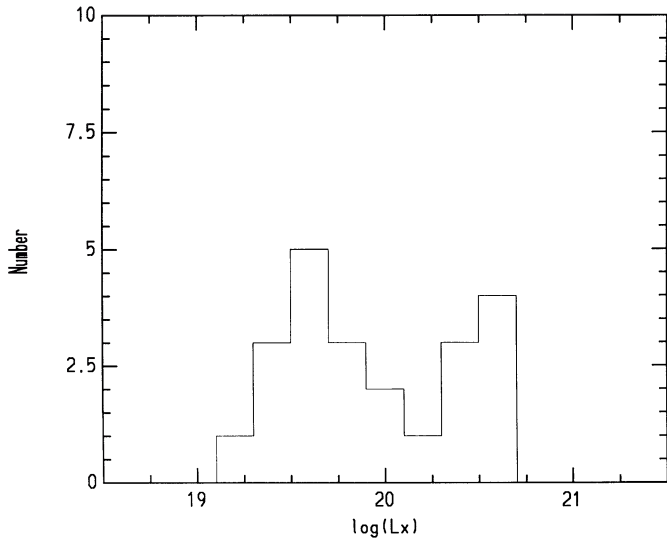


FIG. 3a

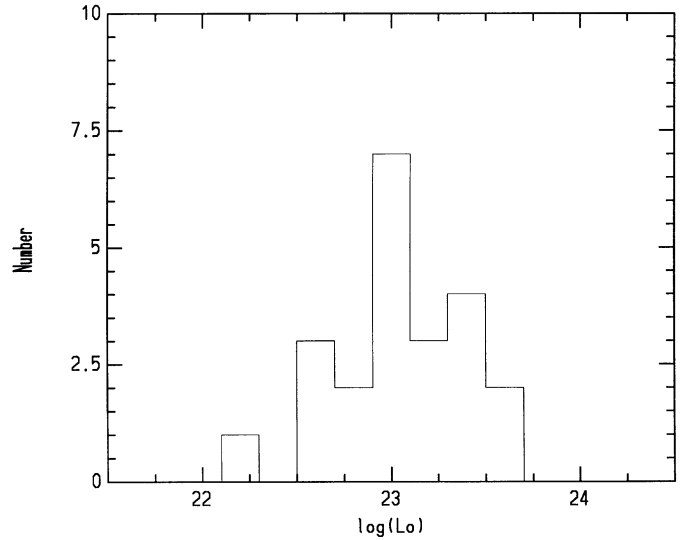


FIG. 3b

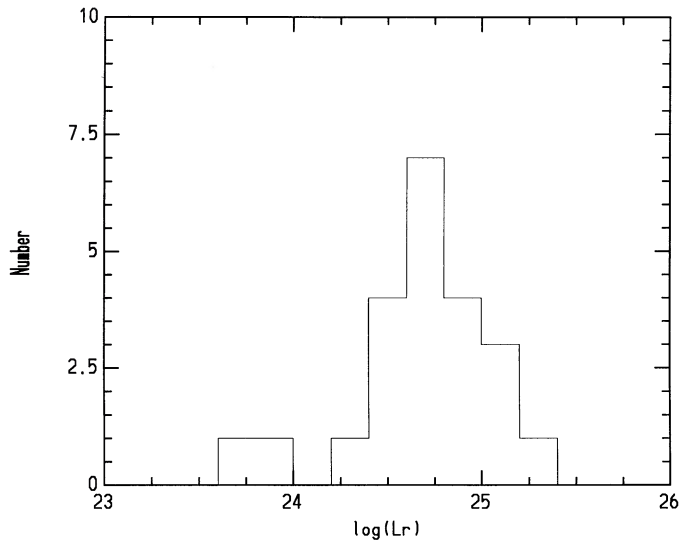


FIG. 3c

FIG. 3.—(a-c) Monochromatic luminosity distributions for the complete EMSS BL Lac sample in the X-ray, optical, and radio. The x-axis is the logarithm of the flux in  $\text{W Hz}^{-1}$ .

of *no* correlation between the variables tested, as estimated using the Kendall  $\tau$ -test (Press et al. 1988). These probabilities are consistent with those derived using the Pearson or the Spearman test. A plot of the correlation between optical and radio luminosities is given as Figure 4. These results are discussed in § 4.2.2.

### 3.3. The Luminosity Function

#### 3.3.1. Calculation

The primary goal of the study described in this paper was the derivation of a luminosity function for a complete sample of BL Lac objects. In essence the derivation of a luminosity function merely requires taking all the objects above a certain luminosity in the sample and dividing that number by the volume surveyed for these objects. Unfortunately, a number of factors make this procedure more complex than it might at first seem. First, the volume surveyed in the EMSS is a function

of flux limit, i.e., as a result of the distribution of IPC exposure times, small areas of sky have been surveyed to quite low fluxes, while a larger area has been surveyed to a higher flux limit (Gioia et al. 1990a; see also Table 6). Second, any evolution in the population being studied would mean that objects at high redshift cannot be simply combined with objects at low redshift.

Fortunately, a procedure for dealing with these problems has been described in some detail by Avni & Bahcall (1980). We follow their procedure for coherent analysis of a set of independent samples. Given a table of object fluxes and redshifts, and another table of sky coverage as a function of limiting flux, the algorithm for estimation of any evolution in a population, and for estimation of a local luminosity function using objects at a variety of redshifts, while also accounting for variable flux limits, is as follows:

1. Coherent analysis assuming density evolution.
  - a) Calculate the objects' luminosities, and then for each object perform the sums described in item *b* below.
  - b) For each flux limit, find the redshift at which the object flux would be equal to the flux limit. Calculate the volume enclosed by this redshift (multiplied by the differential sky

TABLE 5  
CORRELATION ANALYSIS FOR EMSS BL LAC SAMPLE  
FLUXES AND LUMINOSITIES (22 objects)<sup>a</sup>

	FLUXES			LUMINOSITIES		
	$F_o$	$F_r$	$D$	$L_o$	$L_r$	$D$
$F_x$ .....	8	10	50	...	...	...
$F_o$ .....	...	0.02	0.2	...	...	...
$F_r$ .....	...	...	1.2	...	...	...
$L_x$ .....	...	...	...	3.0	2.6	0.4
$L_o$ .....	...	...	...	...	0.9	18
$L_r$ .....	...	...	...	...	...	19

<sup>a</sup> Parameters are the same as those in Table 3, apart from  $D$ , which is the logarithm of the proper distance in meters (for the purposes of the Kendall  $\tau$ -test this is identical to redshift). The table entries are the percentage probability that there is *no* correlation between the variables in the corresponding row and column.

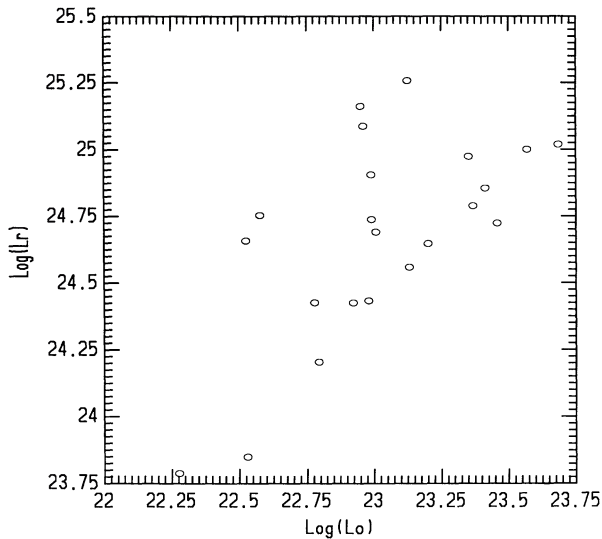


FIG. 4.—Plot of the correlation between the radio and optical luminosities of the complete EMSS BL Lac sample. The axes are the logarithms of the luminosities in  $\text{W Hz}^{-1}$ .

coverage for that limit). When doing the volume integral, include a weighting for density evolution. Add this to the accumulating “available volume” ( $V_a$ ). Also calculate the actual volume enclosed by the object redshift (also multiplied by the differential sky coverage) and add this to the accumulating “enclosed volume” ( $V_e$ ). Note that if the observed object flux is below the current flux limit, the increment to the “enclosed volume” should be calculated using the redshift determined for the “available volume,” and not the object redshift. This procedure is summarized in equations (42) and (43) of Avni & Bahcall (1980):

$$V_a(F) = \sum_i \frac{\Omega_i}{4\pi} V'(z'_{\max}(F)), \quad (2)$$

$$V_e(z, F) = \sum_i \frac{\Omega_i}{4\pi} V'(\min[z, z'_{\max}(F)]). \quad (3)$$

Details of the variable definitions are given in that paper.

TABLE 6  
SKY COVERAGE FOR COMPLETE EMSS  
BL LAC SAMPLE<sup>a</sup>

$F_x^b$	Differential Area <sup>c</sup>	Integral Area <sup>c</sup>
5.0.....	385.90	385.90
5.4.....	36.70	422.60
6.5.....	72.79	495.40
7.8.....	62.98	558.40
9.4.....	45.95	604.40
11.3.....	27.20	631.60
13.5.....	15.95	647.50
16.2.....	7.81	655.30
19.5.....	3.18	658.50
23.4.....	1.38	659.90
28.0.....	0.46	660.40
33.6.....	0.11	660.50
40.4.....	0.02	660.50

<sup>a</sup> North of  $-20^\circ$ ,  $F_x > 5 \times 10^{-13} \text{ ergs cm}^{-2} \text{ s}^{-1}$  (0.3–3.5 keV).

<sup>b</sup> Flux in units of  $1.0 \times 10^{-13} \text{ ergs cm}^{-2} \text{ s}^{-1}$  in the 0.3–3.5 keV band, assuming a spectral index  $\alpha = -1$ .

<sup>c</sup> Areas in square degrees.

c) After performing the above sum for all flux limits, calculate the ratio of  $V_e/V_a$  for the object.

d) After calculating  $V_e/V_a$  for all objects, various statistical tests can be performed to see whether the model for density evolution is consistent with the data. First, the mean of the volume ratios ( $V_e/V_a$ ) should be compared with 0.5, and the rms about that mean compared with that expected for a uniform distribution  $[(12N)^{-0.5}]$ , where  $N$  is the number of objects. Second, one must perform a Kolmogorov-Smirnov test, directly comparing the ratio distribution with a uniform one. This both allows identification of the “best-fit” value for the evolution parameter and also gives error bounds based on the number of data points and their flux and redshift distribution (basically an internal error estimate).

e) If these tests are satisfied, the luminosity function can be calculated using the sum of  $1/(V_a)$  for all objects above a given luminosity.

## 2. Coherent analysis assuming luminosity evolution.

a) The situation for luminosity evolution is only slightly different from that for density evolution. The differences are as follows: In step *a*, the luminosity for each object is that “evolved” to zero redshift. In step *b*, as the maximum redshift is being estimated, the evolving luminosity with redshift must be used. Also, the density weighting in the volume integral must obviously be removed.

A differential luminosity function can be constructed in a similar way to the integral luminosity function by breaking the observed luminosity range into a set of logarithmic bins. For each bin one can count the number of objects falling into it, and calculate the sum of  $1/(V_a)$  for each object in the bin. When divided by the bin width, this gives the density of objects per unit volume per luminosity interval. The uncertainty in each value can be determined from the Poisson uncertainty on the number of objects in the bin.

A program to implement these algorithms was developed, and a number of different evolutionary parameterizations were tested. Table 6 contains the differential sky coverage for the EMSS survey north of  $-20^\circ$  for a source spectral index  $\alpha = -1$  (see Gioia et al. 1990a for details). For the purposes of the complete BL Lac sample, this distribution has been truncated at  $5 \times 10^{-13} \text{ ergs cm}^{-2} \text{ s}^{-1}$  (0.3–3.5 keV). Figures 5a and 5b show the variation of the mean  $V_e/V_a$  with evolution parameter. In Figure 5a, density evolution of the form

$$\rho(z) = \rho(0)(1+z)^\beta \quad (4)$$

was tested with various values for the evolution rate  $\beta$ . A best-fit value of  $\beta = -5.5$  was found with  $\pm 2 \sigma$  limits of  $-9.0$  to  $-1.75$ . In Figure 5b, luminosity evolution of the form

$$L_x(z) = L_x(0)(1+z)^\gamma \quad (5)$$

was tested with various values of the evolution rate  $\gamma$ . A best-fit value of  $\gamma = -7$  was found with  $\pm 2 \sigma$  limits of  $-16.25$  to  $-1.5$ . A Kolmogorov-Smirnov test shows that the  $2 \sigma$  range given above is also the range within which the  $V_e/V_a$  distribution has a greater than 1% chance of being drawn from a uniform distribution with mean of 0.5. The results from the  $V_e/V_a$  analysis are summarized in Table 7. Clearly, the evolution is rather poorly determined, owing to the small number of objects and the fairly small redshift range in the sample. However, our data indicate that there is less than a 1% probability that our sample of BL Lac objects shows zero or posi-

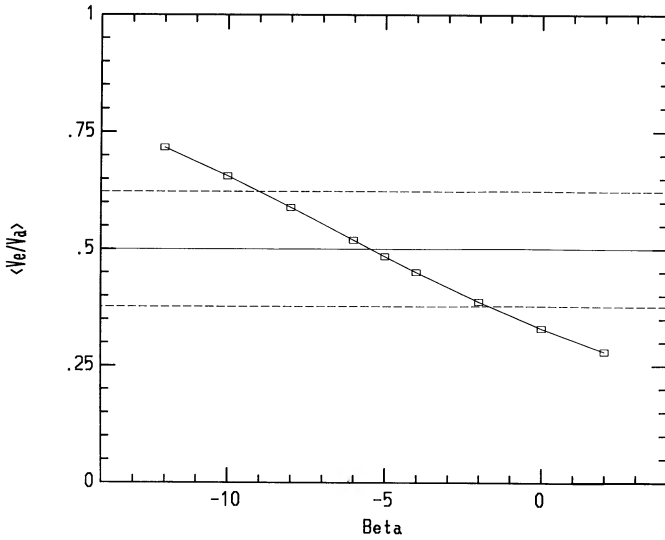


FIG. 5a

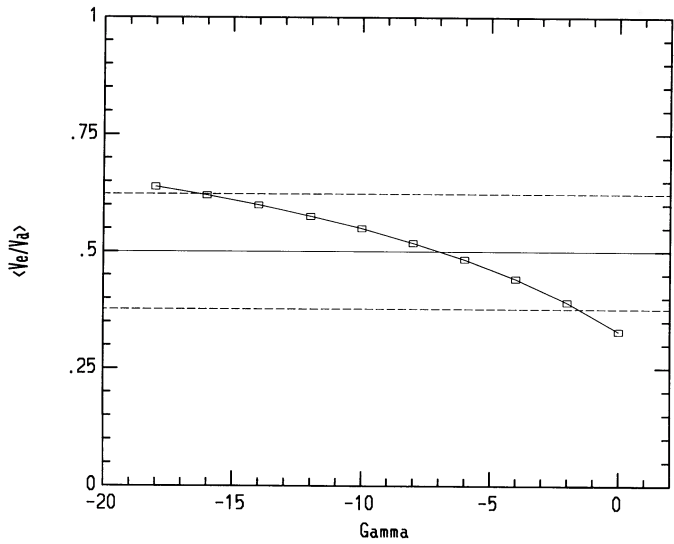


FIG. 5b

FIG. 5.—Variation of mean  $V_e/V_a$ , (a) with density evolution parameter  $\beta$  and (b) with luminosity evolution parameter  $\gamma$ . Solid horizontal line indicates mean = 0.5; dashed lines indicate  $2\sigma$  boundaries. See text.

tive evolution. Our best fit to the data has strong *negative* evolution, i.e., BL Lac objects were either much less common or much less luminous in the recent past.

Figure 6 shows the evolved (i.e.,  $z = 0$ ) luminosity functions derived for the two forms of evolution. (N.B.: The luminosities used in the luminosity function calculation and shown in the figure are *not* the monochromatic values shown in Table 3 but are the broad-band values from the 0.3–3.5 keV band in ergs per second. This is done for computational ease and to allow straightforward comparison with other luminosity functions in the literature.) We should also repeat that the luminosities discussed are calculated assuming that the BL Lac X-ray emission is isotropic. The object luminosity integrated over all lines of sight is unknown, and may be considerably smaller than that predicted by the above assumption. In Figure 7 we show the differential luminosity functions for the same models. Bins which contained no objects are not plotted. These luminosity functions are the result of assuming a value for the evolution parameter and then combining the information from all the EMSS BL Lac objects into a luminosity function at a single redshift. Zero redshift was chosen for this to allow easy comparison with the EMSS AGNs (Maccacaro et al. 1991) and with low-redshift samples of objects such as radio galaxies and clusters of galaxies.

We show the effect of the uncertainty in the evolution parameter in Table 8, where we list the density of BL Lac ( $\text{Mpc}^{-3}$ ) with X-ray luminosity above a given value at  $z = 0$  for the best fit and  $\pm 2\sigma$  limits of the evolution parameter. The luminosity function at redshifts other than zero can be calculated by evolving either the densities in the first part of Table 8 using equation (4) or the luminosities in the second part of Table 8 using equation (5).

TABLE 7  
RESULTS FROM THE  $V_e/V_a$  TEST

Model	Form of Evolution	Best Fit	$2\sigma$ Range
Density evolution .....	$\rho(z) = \rho(0)(1+z)^\beta$	$\beta = -5.5$	-9.0, -1.75
Luminosity evolution ...	$L_x(z) = L_x(0)(1+z)^\gamma$	$\gamma = -7.0$	-16.25, -1.5

We note that the luminosity function evolved to zero redshift produced by the best-fit luminosity evolution predicts objects with very high X-ray luminosities ( $10^{47}$  ergs  $\text{s}^{-1}$  [0.3–3.5 keV]), while the  $-2\sigma$  luminosity evolution case would predict a population of BL Lac objects at zero redshift with luminosities of  $10^{49}$  ergs  $\text{s}^{-1}$  (0.3–3.5 keV). This may indicate that density evolution is the preferred solution on the basis of energetics, although the current best-fit value for the case of luminosity evolution is consistent with the observed number of BL Lac objects found in the Piccinotti et al. (1982) all-sky, high-flux sample of X-ray sources.

3.3.2. Possible Causes of Systematic Errors

The first point to consider is the “serendipitous” nature of the EMSS survey. If the objects found in the EMSS list are

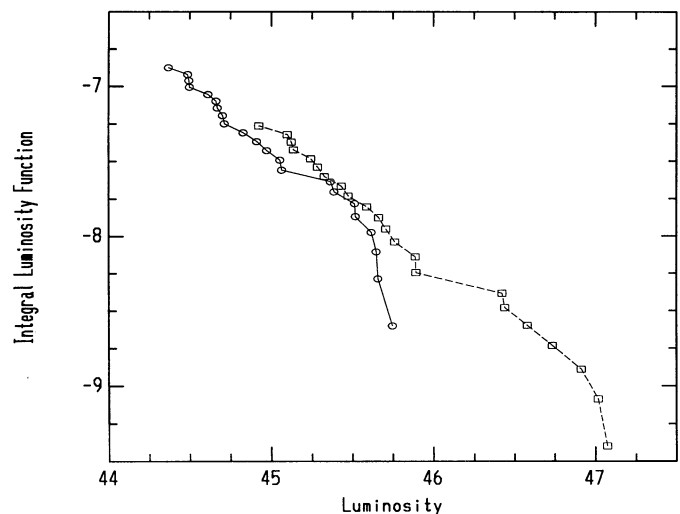


FIG. 6.—EMSS BL Lac luminosity function evolved to  $z = 0$  for density evolution  $\beta = -5.5$  (circles) and luminosity evolution  $\gamma = -7.0$  (squares). Luminosities are the logarithm of the 0.3–3.5 keV value in ergs  $\text{s}^{-1}$ . The y-axis is the number of objects  $\text{Mpc}^{-3}$  with luminosity above the x-axis value at zero redshift.

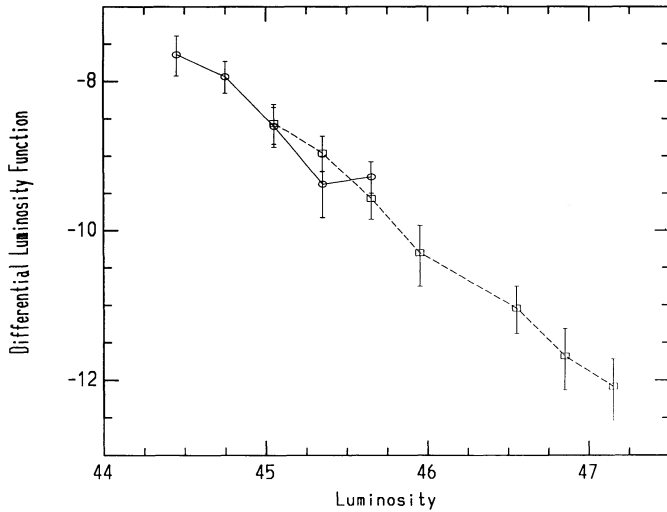


FIG. 7.—EMSS BL Lac differential luminosity function for density evolution  $\beta = -5.5$  (circles) and luminosity evolution  $\gamma = -7.0$  (squares). Luminosities are the logarithm of the 0.3–3.5 keV value in  $\text{ergs s}^{-1}$ . The y-axis is the number of objects  $\text{Mpc}^{-3}$  per luminosity interval of  $10^{44}$   $\text{ergs s}^{-1}$ . A bin size of 0.3 in  $\log$  luminosity was used. The error bars indicate the Poisson uncertainty due to the number of objects in each bin.

actually physically associated with the targets of the IPC observations, a bias can be introduced into the sample. This was discussed in detail in Gioia et al (1990a), where it was shown that none of the identified EMSS sources were associated with the IPC target. Since some of the redshifts of the EMSS BL Lac sample were not known at the time that the Gioia et al. (1990a) paper was being written, we have gone back and specifically rechecked the IPC targets of the EMSS BL Lac exposures for physical association. The targets of the EMSS BL Lac observations included three stars, three galaxies, six clusters of galaxies, nine AGNs/QSOs, and one image of a north ecliptic pole field. None of the extragalactic targets have redshifts that match the EMSS BL Lac value. The closest match was between MS 1235.4+6315 and the cluster Abell 1576, but the redshift difference (corresponding to a velocity difference of  $6000 \text{ km s}^{-1}$ ) is large enough that the two objects seem unrelated. In fact, the serendipitous nature of the EMSS survey, resulting in a low flux limit (i.e., a deep survey) but with widely separated sources, makes the sample *less* susceptible to the fluctuations in source densities that seem to affect the deep “pencil-beam” QSO surveys.

TABLE 8  
INTEGRAL LUMINOSITY FUNCTION (ILF) AT  $z = 0^a$

$\log L_x^b$	DENSITY ILF ( $z = 0^c$ )			LUMINOSITY ILF ( $z = 0^c$ )		
	$\beta = -9.0$	$-5.5$	$-1.75$	$\gamma = -16.25$	$-7.0$	$-1.5$
44.5.....	-6.7	-7.0	-7.4	...	...	-7.4
45.0.....	-7.0	-7.4	-8.1	...	-7.3	-8.0
45.5.....	-7.3	-7.8	-8.4	...	-7.8	-8.5
46.0.....	...	...	...	-7.3	-8.3	...
46.5.....	...	...	...	-7.7	-8.5	...
47.0.....	...	...	...	-8.1	-9.1	...

<sup>a</sup> Shown for various evolutionary parameterizations and for density and luminosity evolution.

<sup>b</sup> Broad-band X-ray luminosity in the 0.3–3.5 keV band in  $\text{ergs s}^{-1}$ .

<sup>c</sup> Integral luminosity function =  $\log$  of the number of BL Lac objects  $\text{Mpc}^{-3}$  with X-ray luminosity above a given value.

Using the global spectral indices, we can investigate whether the negative evolution seen in the EMSS BL Lac objects is an artifact from our spectroscopic classification scheme, due to high-luminosity “BL Lac objects” actually all having strong enough emission lines to be called AGNs. Using the data in Stocke et al. (1991), an  $\alpha_{\text{ox}}$  and  $\alpha_{\text{ro}}$  diagram for the EMSS AGNs with declination greater than  $-20^\circ$  and with X-ray flux greater than  $5 \times 10^{-13} \text{ ergs cm}^{-2} \text{ s}^{-1}$  (0.3–3.5 keV) can be constructed. In such a plot, as shown in Stocke et al. (1991), EMSS BL Lac objects are restricted to a fairly small region. Note that the definition of  $\alpha_{\text{ox}}$  and  $\alpha_{\text{ro}}$  uses the monochromatic optical flux at 2500 Å, while the optical luminosities elsewhere in this paper are referred to 5500 Å. A sample of the AGNs in this part of the diagram can be constructed, and the evolution of a combined sample of AGNs and BL Lac objects calculated, i.e., a sample of EMSS objects with nonthermal emission, chosen for their global energy distribution but with no reference to their emission-line EWs. There are four AGNs in the same part of the  $\alpha_{\text{ox}}$  and  $\alpha_{\text{ro}}$  diagrams as the EMSS BL Lac objects. The same  $V_e/V_a$  test as used above, when run on the combined BL Lac and AGN sample, yields a best-fit density evolution power of  $\beta = -3.7$  with  $2 \sigma$  range  $-7.6$  to  $+0.8$ . Thus inclusion of AGNs with similar global energy distribution but with emission lines that are significantly stronger than our 5 Å criterion gives a sample of objects which still shows evidence for negative evolution, although the no-evolution case is now allowed at the  $2 \sigma$  (5% probability) level.

Another reasonable fear might be that we are systematically getting the redshifts wrong and are putting high- $z$  BL Lac objects at incorrect low  $z$ 's. We can investigate the consequences of this possibility by moving the three BL Lac objects with the most uncertain redshifts (category P in Table 2) to the highest redshift in the sample ( $z = 0.638$ ). If we then rederive the mean  $V_e/V_a$  for density evolution, the best fit and  $2 \sigma$  limits are very little changed ( $\beta = -4.5$  with  $2 \sigma$  range  $-7.8$  to  $-1.0$ ). This result can be understood when it is considered that, if  $k$ -corrections are ignored and zero evolution assumed, the  $V_e/V_a$  test could be run merely using fluxes (for low redshifts or a flat universe). That is, the need for negative evolution could be demonstrated without any redshift information. The significance of the result depends on the fact that a large fraction of the BL Lac objects are found well above the survey flux limit. It is only when the strength of the evolution is required that the redshifts are needed.

What other effects might produce an apparent negative evolution from an actually nonevolving population? Since the high-flux EMSS sample used is fully identified, the only possibility would be that we were misidentifying low-flux BL Lac objects as something else. If AGNs are ruled out, the only alternative left would be misidentification as clusters of galaxies. This point is discussed by Stocke et al. (1989), who showed that it is very unlikely that a significant number of the cluster sources in the EMSS could conceal BL Lac objects.

In summary, we do not feel that our result of negative evolution is due to biases or incorrect identifications in the EMSS.

## 4. DISCUSSION

### 4.1. Models for BL Lac Objects

Before embarking on a discussion of our new results, we should first mention the various models for BL Lac objects which we hope to test.

1. First, it is conceivable that BL Lac objects are an unusual,

isotropically radiating population of objects. This is not a popular view, largely because of the difficulty in explaining the rapid variability and high luminosities of the class with this model.

2. Alternatively, BL Lac objects could be a subset of AGNs in which there is a relativistic jet pointed at the observer. Relativistic beaming can explain many of the properties of BL Lac objects (e.g., see Königl 1989). This explanation leaves open the question of the “parent” population, i.e., the objects with jets misaligned with the observer. Two popular candidates for this population are either radio-loud quasars or low-luminosity radio galaxies (FR I radio galaxies) (see Browne 1989). A complication to this model is that the effects of beaming may be different at different frequencies. For example, Stocke et al. (1985) suggested that the X-ray emission from BL Lac objects may be more nearly isotropic than the radio emission.

3. A third model (Ostriker & Vietri 1990) suggests that BL Lac objects are in fact gravitationally (micro)lensed optically violently variable (OVV) quasars, in which a background OVV quasar is amplified by stars in a foreground galaxy. According to this model the redshifts measured from starlight features in the BL Lac spectra are actually the redshifts of the foreground lensing galaxies. Observations of some radio-selected BL Lac objects support this model (e.g., Stickel, Fried, & Kühn 1989b).

#### 4.2. EMSS BL Lac Redshifts and Luminosities

##### 4.2.1. Sample Comparisons

It is instructive to compare the EMSS BL Lac properties with other objects in the EMSS. A number of essentially complete subsets of the EMSS survey can be constructed for this purpose with the same criteria as the complete BL Lac sample, i.e., by choosing objects with declination greater than  $-20^\circ$  and with X-ray flux greater than  $5 \times 10^{-13}$  ergs  $\text{cm}^{-2}$   $\text{s}^{-1}$  (0.3–3.5 keV) (see Stocke et al. 1991 for details of the optical identification). The first thing to note is that the BL Lac sample has the highest median redshift of the high-flux extragalactic objects (BL Lac objects, AGNs, or clusters; see Table 9). It also has the highest median X-ray luminosity (4 times the cluster median and 9 times the AGN median).

Comparison with other BL Lac objects is difficult, since the EMSS sample is the first one both to be well defined and to have almost complete redshift information. The samples we chose to compare with are the *HEAO 1* sample (Schwartz et al. 1989), an incomplete set of 21 BL Lac objects, 14 with redshifts, selected by their X-ray flux; the 1 Jy sample of Kühn & Schmidt (1990) with 34 objects, 18 with redshifts in the literature, selected by radio flux at 6 cm; and the subsample of radio-selected objects from Ledden & O’Dell (1985) and Maraschi et al. (1986) of 54 objects, 24 with redshifts. The median redshifts and luminosities for the objects with redshifts in each sample are given in Table 9. The first thing to note is that the X-ray luminosities of the three BL Lac samples with X-ray measurements (two X-ray-selected and one radio-selected) are similar, although the EMSS BL Lac objects do have slightly higher median luminosity. This point was noted by Maraschi et al. (1986) for a mixed sample of BL Lac objects and OVV quasars. At the same time, the radio luminosities of the two radio-selected samples are found a factor of 10–100 higher than the X-ray-selected samples.

The conclusion drawn is that, since X-ray surveys do not find a significant number of the “radio-strong” BL Lac objects found in radio surveys, they must be considerably rarer. This conclusion is supported by the relative surface densities. Wolter et al. (1991a) show that the number of X-ray-selected BL Lac objects is leveling off toward an asymptotic value of 0.1  $\text{deg}^{-2}$  below an X-ray flux of  $1.0 \times 10^{-12}$  ergs  $\text{cm}^{-2}$   $\text{s}^{-1}$  in the 0.3–3.5 keV energy band. Based on the BL Lac objects known to be present in the S5 and 1 Jy radio surveys (Kühn & Schmidt 1990) a similar flattening in the radio source counts is observed below 0.75 Jy, at a surface density 10–30 times lower. From pointed *Einstein* observations (Worrall & Wilkes 1990), radio-selected BL Lac objects with radio fluxes of about 1 Jy are known to have X-ray fluxes of about  $1.0 \times 10^{-12}$  ergs  $\text{cm}^{-2}$   $\text{s}^{-1}$ , showing that these flux levels yield comparable depths for typical radio-selected BL Lac energy distributions. Further, since the known redshifts of radio-selected BL Lac objects (e.g., Stickel, Fried, & Kühn 1989a) extend to higher values than the X-ray-selected BL Lac objects in this paper, the implied

TABLE 9  
COMPARISON OF MEDIAN LUMINOSITIES AND REDSHIFT OF THE  
EMSS BL LAC SAMPLE WITH OTHER SAMPLES

Sample	Number of Objects <sup>a</sup>	$z$	$L_x^b$	$L_o^b$	$L_r^b$
EMSS BL Lac <sup>c</sup> .....	22/22	0.30	19.83	22.29	24.72
EMSS AGN <sup>c</sup> .....	140/140	0.13	18.87	22.69	...
EMSS cluster <sup>c</sup> .....	45/45	0.17	19.19	...	...
<i>HEAO 1</i> (Schwartz et al. 1989) .....	21/14	0.06	19.49	22.69	24.58
Radio-selected <sup>d</sup> .....	54/24	0.07	19.41	22.52	25.83
1 Jy (Kühn & Schmidt 1990) .....	34/18	0.37	...	23.93	26.94
3CR FR I (Fabbiano et al. 1984) <sup>e</sup> .....	22/22	0.02	17.31	22.76	24.78 <sup>f</sup>
3 CR FR II (Fabbiano et al. 1984) <sup>e</sup> .....	18/18	0.09	18.32	22.72	25.84 <sup>f</sup>
Elliptical (Fabbiano et al. 1989) <sup>e</sup> .....	50/50	...	16.09	22.35	21.55
S0 (Fabbiano et al. 1989) .....	34/34	...	15.33	22.09	20.39

<sup>a</sup> The first number is the total number of objects in the paper or sample; the second number is the number of objects with a redshift or distance.

<sup>b</sup> Logarithm of the monochromatic luminosity as in Table 3.

<sup>c</sup> Declination  $> -20^\circ$ ,  $F_x > 5 \times 10^{-13}$  ergs  $\text{cm}^{-2}$   $\text{s}^{-1}$  (0.3–3.5 keV).

<sup>d</sup> Radio-selected BL Lac objects from Ledden & O’Dell 1985 and Maraschi et al. 1986.

<sup>e</sup> Upper limits from Fabbiano et al. 1984, 1989 were taken as detections for calculation of the median.

<sup>f</sup> Note: The luminosities at 5 GHz for the 3CR objects are calculated from the luminosity at 178 MHz using spectral indices from the literature.

volume density ratio of X-ray- to radio-selected BL Lac objects is greater than 30. We also note that, since HPQs are a small fraction of any radio-selected blazar sample, these must be rarer still, explaining the current lack of any such objects in the EMSS.

To test the second model described in § 4.1 above, a number of other comparison samples have been constructed. The radio galaxies from Fabbiano et al. (1984) are the best collection of radio galaxy X-ray data available. The luminosities for the FR I and FR II subsets of that paper are also given in Table 9. Note that the radio luminosities tabulated were produced by correcting the 178 MHz total radio luminosities tabulated in Fabbiano et al. (1984) to 5 GHz using spectral indices from the literature. Also in Table 9 are the luminosities of "normal" early-type galaxies from Fabbiano, Gioia, & Trinchieri (1989). Both of the above samples contain a significant fraction of upper limits. For the median calculation these were taken as detections. It can be seen that the X-ray luminosities of FR I galaxies are lower than the EMSS BL Lac objects by a factor of 300, while the FR II galaxies are lower by a factor of 30. Interestingly, there is a very good match between the median radio luminosity of the EMSS BL Lac objects and FR I radio galaxies. We consider this to be strong support for the hypothesis that X-ray-selected BL Lac objects are in fact FR I radio galaxies with their X-ray (and probably optical) continuum emission enhanced by the effects of beaming (see also Wardle, Moore, & Angel 1984).

In the optical, the EMSS BL Lac luminosities are about a factor of 4 brighter than those of elliptical galaxies. We are working on a deconvolution of the starlight and nonthermal contributions to the EMSS BL Lac optical luminosities, but pending that result, it can be said that the data are consistent with the EMSS BL Lac objects residing in galaxies with luminosities in the same range as bright ellipticals together with some additional nonthermal component. Ulrich (1989), using a nearby (largely radio-selected) sample of BL Lac objects, has done such a deconvolution and shows that the host galaxies are well matched in luminosity to the host galaxies of a sample of low-luminosity radio galaxies. In Table 9 the 1 Jy sample of BL Lac objects have higher total optical luminosities, again consistent with the picture described in Stocke et al. (1985) in which radio-selected BL Lac objects have more nonthermal continuum relative to their host galaxies, although the median optical luminosity of the (more heterogeneous) radio-selected sample is actually lower than that of the EMSS BL Lac objects.

To summarize the important points of the luminosity comparisons, all samples of BL Lac objects with measured redshifts have comparable X-ray luminosities, which are much higher than those of X-ray-selected AGNs (selected from the same flux range as our complete sample) or 3CR radio galaxies. X-ray-selected BL Lac objects have considerably lower radio luminosity than radio-selected ones, but are well matched in luminosity to the 3CR FR I radio galaxies. Comparisons in the optical require a separation of stellar and nonstellar contributions to be meaningful, and we will address this in a later paper.

#### 4.2.2. Correlations

In discussing the correlations, we will consider as significant those correlations with a less than 1% probability of arising by chance. Obviously this should not be considered a hard boundary.

The correlation between X-ray luminosity and proper dis-

tance is merely that expected from an X-ray flux-limited sample. However, the correlation between radio and optical luminosities (the next strongest found, and backed up by a similar correlation between radio and optical fluxes) is not explicable as a selection effect. There seems to be a fairly narrow range in both optical and radio luminosity in our sample (hence the correlation between the proper distance and the fluxes), but within that range there is a correlation between the two luminosities. This correlation was also found in a more heterogeneous sample of X-ray-selected BL Lac objects studied by Giommi et al. (1990). Until we have deconvolved the stellar and nonthermal contribution to the optical luminosities any interpretation of this result must remain ambiguous. Either there is a correlation between the host galaxy luminosity and the radio power, or there could be a correlation between the nonthermal components in the optical and the radio—perhaps caused by similar beaming of each wavelength. It is interesting to note that a correlation exists between the nuclear radio emission and the host galaxy magnitude for FR I radio galaxies (Fabbiano et al. 1984). A correlation between the stellar and radio luminosity, if confirmed, would seem to sound the death knell of the lensing model 3 for our sample of BL Lac objects. There is nothing in that model which would predict a correlation between the optical luminosity of the lensing galaxy and the apparent radio luminosity of the lensed BL Lac object.

The correlations between the X-ray and the other luminosities in our sample are not as strong as that between the optical and the radio—a fact which can be interpreted as support for the picture put forward in Stocke et al. (1985), which assumes that the beaming model for BL Lac objects is correct, and that the X-ray-emitting material is moving in a wider cone than the optical or radio. Hence, for X-ray-selected BL Lac objects, the X-ray emission can be strongly boosted, while the optical and radio emission is either weakly beamed or unbeamed. A cartoon of a beam geometry which would produce this effect is given in Figure 5 of Urry & Padovani (1990). All that is required is that the collimation of a beam of relativistic particles increases as a function of distance from the beam origin, and that the local mean frequency of radiation emitted by the beam drops as a function of radius.

#### 4.3. EMSS BL Lac Luminosity Function

Schwartz & Ku (1983) were the first to derive an X-ray luminosity function for BL Lac objects based on an incomplete sample of objects. The most recent attempt was that of Padovani & Urry (1990). Our new results are similar to theirs if zero evolution is assumed, but the best-fit  $\beta = -5.5$  density evolution results in a considerably higher zero-redshift luminosity function (by a factor of 6–10). There has been no published attempt to date to produce a luminosity function for radio-selected BL Lac objects,<sup>7</sup> owing to the lack of a complete sample and the small fraction of objects with redshifts. Browne (1983) estimated that the local space density of BL Lac objects with extended radio luminosity greater than  $10^{23.5} \text{ W Hz}^{-1}$  at

<sup>7</sup> After this paper was submitted we received a preprint from Stickel et al. (1991) describing the derivation of a luminosity function for a sample of 34 flat radio spectrum objects with rest EW < 5 Å. They find evidence for positive evolution (radio-selected BL Lac objects more common or more luminous in the past), and derive a luminosity function which predicts  $\log(\text{density of BL Lac objects with radio luminosity } 6 \times 10^{31} < P_{5 \text{ GHz}} < 3.4 \times 10^{34} \text{ ergs s}^{-1} \text{ Hz}^{-1}) = -7.4 (\text{Mpc}^{-3})$  at  $z = 0$ .

1.4 GHz was  $2 \times 10^{-8} \text{ Mpc}^{-3}$  or higher, using essentially the same sample as Schwartz & Ku (1983).

Wolter et al. (1991a) compared three basic beaming models with the EMSS number count data. The first was simply the result of beaming a single-power-law intrinsic luminosity function. As described in Urry & Shafer (1984), this results in an observed luminosity function with a flatter slope than the intrinsic one at low luminosities, with a break to the intrinsic slope above a certain luminosity. This model was used to show that a flattening in the number counts of objects as one goes to fainter fluxes could be produced by a beamed luminosity function, *without* the need for negative evolution. However, our new complete redshift information suggests strongly that negative evolution is present, and so beaming alone is of less interest. The second model considered was that of Padovani & Urry (1990), who calculated the luminosity function of FR I radio galaxies using the data from Fabbiano et al. (1984), and from that calculated the predicted BL Lac luminosity function assuming a fairly simple beaming model with FR I radio galaxies as the host population (i.e., model 2 in § 4.1 above). Unfortunately, the uncertainty in the exact value for the evolution for our BL Lac sample (and the form—density or luminosity) causes considerable uncertainty in the derived zero-redshift luminosity function, as can be seen from Table 8. For the purposes of comparison, we will adopt the best-fit evolution values. These luminosity functions are shown in Figure 8a. As can be seen, the model is too low for our best-fit luminosity function by a factor of 6–10, although it would fit a zero-evolution luminosity function quite well. Obviously a number of parameters in their model could be adjusted. First, some account can be taken of the probable strong negative evolution in the BL Lac population. Padovani & Urry (1990) considered the effects of positive evolution, but did not discuss negative evolution, which would have the effect of improving their fit to our luminosity function. Also, their parameters  $L_{\text{max}}$

and  $R_{\text{max}}$  could be adjusted to improve the match. The third model considered (and rejected) by Wolter et al. (1991a) assumed that the observed number counts were produced by beamed AGNs. As was clear even with the incomplete redshift information available at that time, this possibility can be ruled out.

Unfortunately, it is less straightforward to evaluate the constraints imposed on the lensing model (model 3 in § 4.1 above) by the observed luminosity function, since no detailed predictions have been produced for the luminosity function of BL Lac objects in any wave band for this model (Ostriker & Vietri 1990). The strong negative evolution suggested by Maccacaro et al. (1984b) and found in this paper has been explained in that model by showing that the redshift distribution of lensing galaxies should have two clear maxima, one at low redshift (around 0.05) and one at high redshift (around 1.6) for an OVV quasar at redshift 2. However, it remains to be seen whether the model can reproduce the observed redshift distribution from some reasonable OVV quasar sample. They do not specify in their paper the expected relative numbers of galaxies in each of the two maxima, but the apparent lack of any BL Lac objects (or in the lensing model, galaxies along the line of sight) with redshift over 0.7 in our sample may be a problem for this model.

The most interesting result from the  $V_e/V_a$  analysis is the confirmation of previous claims of zero or negative evolution of BL Lac number or luminosity with cosmic epoch (Maccacaro et al. 1984b, 1989; Wolter et al. 1991a). This is definitely inconsistent with the evolution found for X-ray-selected AGNs (Maccacaro, Gioia, & Stocke, 1984a; Maccacaro et al. 1991). The found a best-fit luminosity evolution for the EMSS AGNs of  $\gamma = +2.56$  with  $2\sigma$  range of 2.19–2.88, i.e., AGNs more luminous in the past. Optical and radio quasar samples also find strong positive evolution (e.g., see Boyle, Shanks, & Peterson 1988; Peacock & Miller 1988). From our

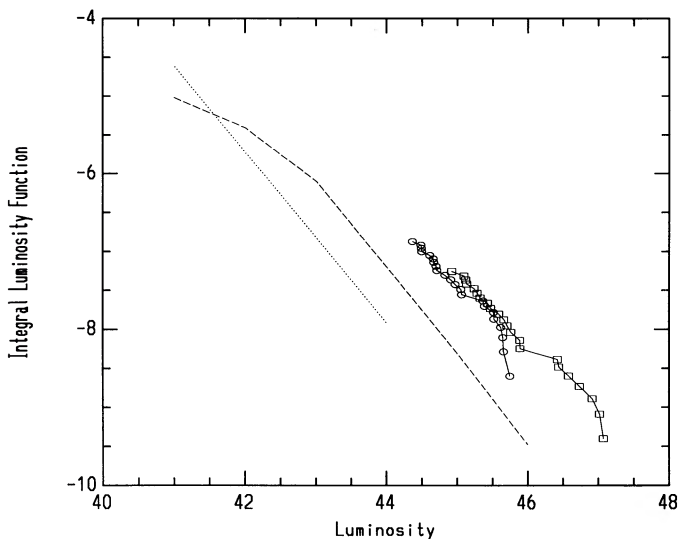


FIG. 8a

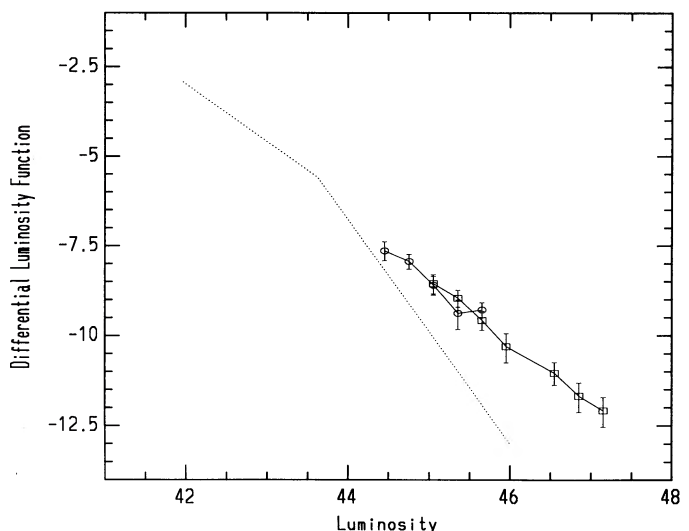


FIG. 8b

FIG. 8.—Comparison of the EMSS BL Lac best-fit luminosity functions for density and luminosity evolution with the luminosity functions of the following (a) FR I radio galaxies and a beaming model from Padovani & Urry (1990). *Dotted line*: luminosity function for FR I radio galaxies; *dashed line*: beaming model prediction for BL Lac objects; *circles connected with solid line*: best-fit luminosity function for the EMSS BL Lac objects with density evolution; *squares connected with solid line*: the same for luminosity evolution. (b) EMSS AGNs (Maccacaro et al. 1991). *Dotted line*: differential luminosity function for EMSS AGNs for the best-fit luminosity evolution of  $\gamma = +2.56$ ; *circles connected with a solid line*: best-fit differential luminosity function for the EMSS BL Lac objects with density evolution; *squares connected with solid lines*: the same for luminosity evolution.

BL Lac data there is no strong reason to prefer density or luminosity evolution. Certainly the difference in the sense of the evolution from that of AGNs and quasars means that carrying over the result for those objects, i.e., that luminosity evolution is preferred over density evolution, would be unjustified. For comparison at  $z = 0$ , the EMSS AGN differential luminosity function can be taken from Maccacaro et al. (1991). Figure 8*b* compares the differential luminosity functions, showing that the EMSS BL Lac objects have a higher space density at high luminosities, but a slightly flatter slope, suggesting that if the BL Lac luminosity function were extrapolated to lower luminosities, the AGN luminosity function would eventually predominate. This, combined with the negative evolution, means that BL Lac objects are not a strong contributor to the X-ray background. Assuming luminosity evolution (for ease of calculation) with  $\gamma = -7$ , and integrating the BL Lac contribution to  $z = 3$ , we find that the BL Lac objects contribute only 3%–4% of the total soft X-ray background (i.e., one-tenth of the AGN contribution found by Maccacaro et al. 1991).

In a similar vein, the differential luminosity function can be compared with that of EMSS clusters of galaxies at low  $z$  in Gioia et al. (1990*b*). Quite similar space densities are found in the region of overlap in luminosity, although we should emphasize that the physical mechanism producing the X-ray emission is probably very different. At low redshift, the X-ray emission from clusters is often resolved, even at the resolution of the IPC, while the EMSS BL Lac objects are not (Stocke et al. 1991). Many more clusters of galaxies than BL Lac objects are found in the EMSS because the luminosity function for clusters extends to much lower luminosities. The decrease in density of high-luminosity clusters found at high redshift (Gioia et al. 1990*b*) is in the same sense as the evolution found for the BL Lac objects. This last fact is of interest because, in the model of Stocke & Perrenod (1981), BL Lac objects were said only to be in clusters in which the central density exceeded a certain value. Unfortunately, the most recent models for the evolution of the intercluster medium (ICM) (Evrard 1990) now suggest that the ICM density evolves very little in a rich cluster between  $z = 1$  and  $z = 0$ , and so the underlying assumption, that BL Lac objects were produced by ram pressure stripping in the ICM which was growing rapidly denser with cosmological epoch, may no longer be acceptable. An alternative mechanism for producing the evolution of AGN properties in clusters of galaxies was described by Roos (1985), where it was suggested that the rate of galaxy mergers in clusters of galaxies is a strong function of epoch.

Approaching the problem from another angle, we note that FR I radio galaxies (a possible host population for BL Lac objects) are found preferentially in high galactic density regions (Prestage & Peacock 1988). A consistent picture can be constructed by incorporating the work of Ellingson, Yee, & Green (1991), who claim that the rapid decline in radio-loud quasars that they see in clusters of galaxies (which occurs between redshifts of 0.6 and 0.4) may be due to a change in the appearance of the AGN from a quasar to a radio galaxy. That is, the quasars seen in the centers of rich clusters at high redshift may become the FR I radio galaxies which make up the host population of our BL Lac objects, and the redshift at which this changeover occurs is reasonably well matched to the redshift at which our BL Lac population is appearing. This leaves unanswered the question of what causes the quasars in clusters to diminish so rapidly in optical magnitude at  $z \sim 0.5$ . We have

started a program of CCD imaging in order to test whether X-ray-selected BL Lac objects are indeed found in clusters of galaxies, and until that is completed, the above must remain speculation.

## 5. CONCLUSIONS

To summarize:

1. We have obtained redshifts for nearly all of an X-ray flux-limited sample of BL Lac objects.
2. With these we can derive the object luminosities, and we find a correlation between the optical and radio luminosities.
3. We can also determine the evolution of these objects, and find strong evidence that they were either fainter or less common per comoving volume at earlier times.
4. We derive integral and differential luminosity functions for our sample.

From these data we can make the following statements concerning the three models describes in § 4.1: (1) BL Lac objects are rare, isotropic emitters; (2) BL Lac objects are relativistically beamed radio galaxies or quasars; (3) BL Lac objects are microlensed quasars.

1. Model 1 makes no detailed predictions of the objects' luminosity or their luminosity functions, and so, until some modeling is done, little can be said about it.
2. Model 2 does make a number of predictions, and it seems to be consistent with the data, if the host population of BL Lac objects is assumed to be FR I radio galaxies comparable in radio luminosity to the 3CR sample, and if the "negative" evolution detected in this sample is taken into account.
3. Model 3 has not yet been explored in sufficient detail to compare with our luminosity function, but qualitatively one would expect a sizable fraction of our BL Lac objects to have no measurable redshift (high- $z$  lenses). The observed correlation between optical and radio luminosities is also a problem for this model.

In our sample we do not find BL Lac objects with the radio luminosities found in the radio-selected samples. This, combined with their similar X-ray luminosity, suggests that the very radio-loud BL Lac objects are much rarer objects. This inference is supported by the relative surface densities at the observed turnover in the X-ray and radio number counts.

There are two possible explanations for the observed differences between X-ray- and radio-selected samples of objects. It is possible (as suggested by Stocke et al. 1985) that the cone into which the X-ray emission is beamed has a larger opening angle than the cone for the radio emission, and that X-ray selection is therefore finding "off-axis" BL Lac objects. Another possibility is that the two selection techniques find intrinsically different objects. We suggest that X-ray selection is proving efficient at finding the beamed subset of FR I radio galaxies, while radio selection may pick up both this class along with the beamed subset of radio-loud quasars, and also cases of microlensing. Both of the above effects would explain the larger fraction of starlight in the X-ray-selected objects.<sup>8</sup> The large sample of BL Lac objects which can be drawn from the *ROSAT* all-sky survey will almost certainly be able to determine which of the above effects dominates. In practice, we

<sup>8</sup> These effects would also explain the recent suggestion of different (positive) evolution for radio-selected BL Lac objects (Stickel et al. 1991).

think it likely that both of the above effects are important. Thus X-ray selection may prove to be a good way of defining a "pure" sample of beamed FR I radio galaxies, while radio selection finds both more extreme beamed FR I galaxies, and also examples of beamed OVV quasars and microlensed quasars. If the above speculations are correct, the "blazar" category is actually a mix of several intrinsically different objects.

The strong negative evolution we find is in the same sense as that found for high-luminosity X-ray-selected clusters of galaxies. It also seems to occur at a redshift which matches the time of disappearance of radio-loud quasars in clusters of galaxies. This all fits together into a (speculative) picture in which

quasars in high-redshift clusters of galaxies evolve into low-luminosity radio galaxies at the present epoch. These radio galaxies are the host population from which the BL Lac objects we have found are the beamed examples.

We would like to thank Meg Urry, Buell Jannuzi, and Wal Sargent for useful conversations. S. L. M. is funded through NASA contract NAS 5-30101. J. S. acknowledges support through NSF grant AST 87-15983 and NASA grant NAG 5-1224. Work on the EMSS at CfA is supported by NASA grant NAS 8-30751 and the Scholarly Studies Program grant SS 88-03-87.

## APPENDIX

This Appendix contains comments on the spectra shown in Figure 1, and on the redshifts given in Table 2. The lines listed after the object name are the features used to estimate the redshift. The letters before each object name refer to the panels in Figure 1.

- (A) MS 0122.1 + 0903; Ca II, G band, Balmer, Mg *b*, Na D.  
 (B) MS 0158.5 + 0019; Ca II, G band, Mg *b*, Na D.  
 (C) MS 0205.7 + 3509; [O II]?, Ca II, Mg *b*, Na D? The spectrum is very featureless.  
 (D) MS 0257.9 + 3429; Ca II, G band, Mg *b*, Na D.  
 (E) MS 0419.3 + 1943; Ca II, Mg *b*? The features are quite strong, but the object is very faint. An MMT spectrum is consistent with the Palomar redshift.  
 (F, G) MS 0607.9 + 7108; Ca II, G band, Mg *b*, Na D. The object was observed twice. It has a close stellar companion. In 1988 November the slit was oriented to exclude the companion, but some light from it may have leaked in. In 1989 April the slit was oriented to include the companion, and unfortunately the spectra were inseparably blended so the objects could not be extracted separately.  
 (H, I) MS 0737.9 + 7441; Ca II, G band, Mg *b*, Na D. The object was observed twice and the spectra agree.  
 (J, K) MS 0922.9 + 7459; Ca II, G band, Mg *b*? The object was observed twice, but is faint. The spectra are consistent, with a break at 6500 Å which is fairly strong and present in both spectra. The ID for this field is confused by the fact that there is a nearby faint AGN with  $z = 1.379$  and a foreground cluster of galaxies (Abell 786) at  $z = 0.124$ .  
 (L, M) MS 0950.9 + 4929. The object was observed twice. The spectrum is featureless in the first exposure. The second epoch has a bump which is on the join between red and blue data and hence is unreliable. There are no stellar absorption features. It has a companion galaxy with  $z = 0.207$ . For the luminosity function calculations its redshift is *assumed* to be the same as that of the companion galaxy.  
 (N) MS 0958.9 + 2102; Ca II, G band, Mg *b*. An MMT spectrum supports this redshift.  
 (O) MS 1207.9 + 3945; Ca II, G band, Mg *b*? The three features match up for consistent  $z$ , but the signal-to-noise ratio is only modest even after 3 hr. Both MMT data, and MCSP data taken at Palomar support this redshift (Stocke et al. 1985).  
 (P) MS 1221.8 + 2452; Ca II, Mg *b*? The features are of marginal significance, and they do not line up perfectly. The redshift is very uncertain.  
 (Q) MS 1402.3 + 0416. The bump starting around 5000 Å is very suggestive of a Ca II break, but it occurs on the join of blue and red data and could just be a scaling problem. The lack of corresponding Mg *b* or Na D throws further doubt on this redshift assignment.  
 (R) MS 1407.9 + 5954; Ca II, G band, Mg *b*, Na D.  
 (S) MS 1443.5 + 6349; Ca II, G band, Mg *b*, Na D.  
 (T) MS 1458.8 + 2249; Ca II, G band, Mg *b*? The spectrum is very featureless, and so despite the good signal-to-noise, the redshift is uncertain.  
 (U) MS 1534.2 + 0148; Ca II, G band, Mg *b*, Na D.  
 (V) MS 1704.9 + 6046; Ca II, G band, Mg *b*, Na D. The spectrum is rather noisy, but the redshift is secure and in good agreement with a previous MMT spectrum.  
 (W, X) MS 1757.7 + 7034; Ca II, G?, Mg *b*, Na D? This object was observed twice. The spectra have different signal-to-noise due to (a) a wider slit being used in 1989 June, (b) better seeing in 1989 June, and (c) more starlight in the larger aperture. Given the above, the spectra are consistent although rather featureless. An MMT spectrum is also consistent with the redshift.  
 (Y, Z) MS 2143.4 + 0704; Ca II, G band, Mg *b*, Na D. This object was observed twice. The comments for MS 1757.7 + 7034 about the signal-to-noise difference apply to this object also.

## REFERENCES

- Avni, Y., & Bahcall, J. N. 1980, ApJ, 235, 694  
 Boyles, B., Shanks, T., & Peterson, B. 1988, in Optical Surveys for Quasars, ed. P. Osmer, A. Porter, R. Green, & C. Foltz (ASP Conf. Proc., Vol. 2; San Francisco: ASP), 1  
 Browne, I. W. A. 1983, MNRAS, 204, 23P  
 ———, 1989, in BL Lac Objects, ed. L. Maraschi, T. Maccacaro, & M. Ulrich (Berlin: Springer-Verlag), 401  
 Ellingson, E., Yee, H. K. C., & Green, R. F. 1991, ApJ, 371, 49

- Elston, R., Jannuzi, B., & Smith, P. 1989, in *BL Lac Objects*, ed. L. Maraschi, T. Maccacaro, & M. Ulrich (Berlin: Springer-Verlag), 253
- Evrard, A. E. 1990, *ApJ*, 363, 349
- Fabbiano, G., Gioia, I. M., & Trinchieri, G. 1989, *ApJ*, 347, 127
- Fabbiano, G., Miller, L., Trinchieri, G., Longair, M., & Elvis, M. 1984, *ApJ*, 277, 115
- Gioia, I. M., Henry, J. P., Maccacaro, T., Morris, S. L., Stocke, J. T., & Wolter, A. 1990b, *ApJ*, 356, L35
- Gioia, I., Maccacaro, T., Schild, R., Wolter, A., Stocke, J., Morris, S., & Henry, J. P. 1990a, *ApJS*, 72, 567
- Giommi, P., Barr, P., Garilli, B., Maccagni, D., & Pollock, A. M. T. 1990, *ApJ*, 356, 432
- Jannuzi, B. 1990, Ph.D. thesis, Univ. of Arizona
- Königl, A. 1989, in *BL Lac Objects*, ed. L. Maraschi, T. Maccacaro, & M. Ulrich (Berlin: Springer-Verlag), 321
- Kühr, H., & Schmidt, G. 1990, *AJ*, 99, 1
- Ledden, J. E., & O'Dell, S. L. 1985, *ApJ*, 298, 630
- Maccacaro, T., Della Ceca, R., Gioia, I. M., Morris, S. L., Stocke, J. T., & Wolter, A. 1991, *ApJ*, 374, 117
- Maccacaro, T., Gioia, I. M., Maccagni, D., & Stocke, J. T. 1984b, *ApJ*, 284, L23
- Maccacaro, T., Gioia, I. M., Schild, R. E., Wolter, A., Morris, S. L., & Stocke, J. T. 1989, in *BL Lac Objects*, ed. L. Maraschi, T. Maccacaro, & M. Ulrich (Berlin: Springer-Verlag), 222
- Maccacaro, T., Gioia, I., & Stocke, J. 1984a, *ApJ*, 283, 486
- Maccacaro, T., Gioia, I. M., Wolter, A., Zamorani, G., & Stocke, J. T. 1988, *ApJ*, 326, 680
- Maraschi, L., Ghisellini, G., Tanzi, E. G., & Treves, A. 1986, *ApJ*, 310, 325
- Maraschi, L., Maccacaro, T., & Ulrich, M., eds. 1981, *BL Lac Objects* (Berlin: Springer-Verlag)
- Ostriker, J. P., & Vietri, M. 1990, *Nature*, 344, 45
- Padovani, P., & Urry, C. M. 1990, *ApJ*, 356, 75
- Peacock, J. A., & Miller, L. 1988, in *Optical Surveys for Quasars*, ed. P. Osmer, A. Proter, R. Green, & C. Foltz (ASP Conf. Proc., Vol. 2; San Francisco: ASP), 194
- Piccinotti, G., Mushotzky, R., Boldt, E., Holt, S., Marshall, F., Serlemitsos, P., & Shafer, R. 1982, *ApJ*, 253, 485
- Press, W. H., Flannery, B. P., Teukolsky, S. A., & Vetterling, W. T. 1986, *Numerical Recipes* (Cambridge: Cambridge Univ. Press)
- Prestage, R. M., & Peacock, J. A. 1988, *M.N.R.A.S.*, 230, 131
- Roos, N. 1985, *ApJ*, 294, 486
- Schwartz, D. A., Brissenden, R. J. V., Tuohy, I. R., Feigelson, E. D., Hertz, P. L., & Remillard, R. A. 1989, in *BL Lac Objects*, ed. L. Maraschi, T. Maccacaro, & M. Ulrich (Berlin: Springer-Verlag), 209
- Schwartz, D., & Ku, W. 1983, *ApJ*, 266, 459
- Stickel, M., Fried, J. W., & Kühr, H. 1989a, *A&AS*, 80, 103
- , 1989b, in *BL Lac Objects*, ed. L. Maraschi, T. Maccacaro, & M. Ulrich (Berlin: Springer-Verlag), 222
- Stickel, M., Padovani, P., Urry, C. M., Fried, J. W., & Kühr, H. 1991, *ApJ*, 374, 431
- Stocke, J., Liebert, J., Schmidt, G., Gioia, I., Maccacaro, T., Schild, R., Maccagni, D., & Arp, H. 1985, *ApJ*, 298, 619
- Stocke, J. T., Morris, S. L., Gioia, I. M., Maccacaro, T., Schild, R. E., & Wolter, A. 1989, in *BL Lac Objects*, ed. L. Maraschi, T. Maccacaro, & M. Ulrich (Berlin: Springer-Verlag), 242
- , 1990, *ApJ*, 348, 141
- Stocke, J. T., Morris, S. L., Gioia, I., Maccacaro, T., Schild, R. E., Wolter, A., Fleming, T. A., & Henry, J. P. 1991, *ApJS*, 76, 813
- Stocke, J., & Perrenod, S. 1981, *ApJ*, 245, 375
- Ulrich, M. 1989, in *BL Lac Objects*, ed. L. Maraschi, T. Maccacaro, & M. Ulrich (Berlin: Springer-Verlag), 45
- Urry, C. M., & Padovani, P. 1990, in *Variability of Active Galactic Nuclei*, ed. H. R. Miller & P. J. Wiita, in press.
- Urry, C. M., & Shafer, R. A. 1984, *ApJ*, 280, 569
- Wardle, J. F. C., Moore, R. L., & Angel, J. R. P. 1984, *ApJ*, 279, 93
- Wills, B. J. 1989, in *BL Lac Objects*, ed. L. Maraschi, T. Maccacaro, & M. Ulrich (Berlin: Springer-Verlag), 109
- Wolfe, A. M., ed. 1978, *Pittsburgh Conf. on BL Lac Objects* (Pittsburgh: Univ. Pittsburgh)
- Wolter, A., Gioia, I. M., Maccacaro, T., Morris, S. L., & Stocke, J. T. 1991a, *ApJ*, 369, 314
- Wolter, A., et al. 1991b, in preparation
- Worrall, D. M., & Wilkes, B. J. 1990, *ApJ*, 360, 396